Bayesian network inference modeling identifies TRIB1 as a novel regulator of cell cycle progression and survival in cancer cells

Rina Gendelman[1], **Heming Xing**[2], **Olga K. Mirzoeva**[1], **Preeti Sarde**[3], **Christina Curtis**[4], **Heidi S. Feiler**[5], **Paul McDonagh**[6], **Joe W. Gray**[5], **Iya Khalil**[7], and **W. Michael Korn**[1,8]

[1]Divisions of Gastroenterology and Hematology/Oncology, Department of Medicine, University of California, San Francisco, CA

[2]Novartis Institutes for BioMedical Research, Inc., Cambridge, MA

[3]Pharmacyclics, Sunnyvale, CA

[4]Departments of Medicine and Genetics, School of Medicine, Stanford University, Stanford, CA

[5]Oregon Health and Sciences University, Portland, OR

[6]Alexion Pharmaceuticals, Lexington, MA

[7]GNS Healthcare, Cambridge, MA

[8]Helen Diller Family Comprehensive Cancer Center, University of California San Francisco, CA

Abstract

Molecular networks governing responses to targeted therapies in cancer cells are complex dynamic systems that demonstrate non-intuitive behaviors. We applied a novel computational strategy to infer probabilistic causal relationships between network components based on gene expression. We constructed model comprised of an ensemble of networks using multi-dimensional data from cell line models of cell cycle arrest caused by inhibition of MEK1/2. Through simulation of reverse-engineered Bayesian network model, we generated predictions of G1-S transition. The model identified known components of the cell cycle machinery, such as CCND1, CCNE2, and CDC25A, as well as revealed novel regulators of G1-S transition, IER2, TRIB1, TRIM27. Experimental validation of model predictions confirmed 10 out 12 predicted genes to have a role in G1-S progression. Further analysis showed that TRIB1 regulated the cyclin D1 promoter via NFκB and AP-1 sites and sensitized cells to TNF-Related Apoptosis-Inducing Ligand (TRAIL)-induced apoptosis. In clinical specimens of breast cancer, TRIB1 levels correlated with expression of NFκB and its target genes (*IL8, CSF2*), and TRIB1 copy number and expression were predictive of clinical outcome. Together our results establish a critical role of TRIB1 in cell cycle and survival that is mediated via the modulation of NFkB signaling.

[5]Corresponding author: W. Michael Korn, M.D., Professor of Medicine, UCSF Divisions of Gastroenterology and Hematology/ Oncology, Department of Medicine, Helen Diller Family Comprehensive Cancer Center, 2340 Sutter St., Box 1387, San Francisco, CA 94115, USA, Phone office: (415) 502 2844, Michael.Korn@ucsf.edu.

Keywords

Molecular network biology; MEK; cell cycle regulation; apoptosis; TRIB1; NFκB

The RAF-MEK-ERK signaling network is a key module of cellular signal integration and transcriptional regulation. Extracellular stimuli (i.e. growth factors, cytokines, chemokines, integrins, etc.) lead to activation of this network bringing on changes in global gene expression and cellular outcomes, such as cell growth, proliferation, migration, and survival. Much research has been focused on the role of Mitogen-Activated Protein Kinase (MAPK) pathway in cancer progression and multiple MEK1/2 inhibitors have been developed and tested in the clinic with limited success as single agents (1,2). It has been well documented by others and our previous work that in cell line models of breast cancer, inhibition of MEK results in cell cycle arrest but not cell death (3,4). We have previously reported activation of a feedback-loop leading to Epidermal Growth Factor receptor (EGFR)-dependent upregulation of Phosphatidyl Inositol 3-Kinase (PI3K) signaling in response to MEK1/2 inhibition (3). This feedback mechanism contributes to resistance to MEK inhibitor-induced apoptosis in these cells.

The MEK-PI3K feedback mechanism highlights the complexities of signal transduction networks that govern non-intuitive responses of cellular systems to pharmacological inhibitors. Reliable network models would be important to make predictions about network responses to signal transduction inhibitors. This would allow to efficiently identify key network nodes that could be targeted therapeutically, in particular as part of combination therapies. Various modeling technologies have emerged that capture network complexities in different ways (5). Among those, Bayesian network inference models are particularly promising since they are not only capable of predicting complex network structures but also suggest directionality of interactions between network nodes, which leads to *in silico* hypotheses generation (6,7).

In order to build a model of transcriptional and cellular responses to MEK inhibition, we assessed time-dependent changes in mRNA expression profiles and cell cycle distribution following MEK inhibition in breast cancer cells. Using a novel Bayesian network inference computational engine (6), ensembles of networks were calculated that revealed novel MEK-dependent regulators of the cell cycle and suggested so far unknown mechanisms of pathway cross-talk with the NFκB network. These model predictions were experimentally validated in cell culture models and demonstrate a role of one of the MEK-regulated genes, *TRIB1*, in mediating cross-talk with the NFκB network. Further analyses in a large cohort of human breast cancers provided evidence for the existence of a TRIB1-NFκB network in tumors and revealed *TRIB1* as a predictor of breast cancer-free survival.

Materials and Methods

Reagents

The following reagents were used: U0126 (Promega), epidermal growth factor (EGF; Millipore), mimosine (Sigma), rhTRAIL (Millipore), rhTNFα (Life Tech), TriplePrep Kit

(GE-Healthcare). ON-TARGET plus SMARTpools siRNAs, NC (non-coding negative control oligos) and individual oligos constituting the pools were purchased from Dharmacon. RNAiMax and Lipofectamine LTX transfection reagents were from Invitrogen. Antibodies: αR-TRIB1 (Millipore), αR-CCND1, αM-CCNA2, αR-CDC25A, αR-IER2, αR-pCDK2, αR-pIKKa (Santa Cruz Biotechnology), αM-FLIP (Enzo Life Sciences), αM-BID (BD Biosciences), αM-DR5 (R&D Systems), all other antibodies were from Cell Signaling Technologies.

DNA Constructs

The TRIB1-EGFP construct was a generous gift from Dr. Kiss-Toth. The cyclin D1 promoter-containing construct pD1luc WT and mutant promoter constructs D1-κB1/2m, harboring two point mutations in the D1-κB1 (CGCG<u>A</u>CCCCC) and the D1-κB2 (CG<u>C</u>GAGTTTT) binding site (introduced point mutations are underlined), were a gift from Dr. Hinz (Max-Delbrück-Center for Molecular Medicine, Berlin, Germany). AP-1 mutant (AP1m) and EtsA/EtsB double mutant (EtsA/Bm) CCND1 promoter constructs were generated by site-directed mutagenesis of pD1LucWT construct. NFkB-Luc, pMetLuc-C vector, SEAP vector reporter constructs were from Clontech.

NFκB promoter reporter assay

Cells were co-transfected with 500ng of NFκB -Luc and 250ng of SEAP transfection-control vectors for 18 hours then treated with 10ng/ml TNFα. Activation of NFκB promoter was assayed using Ready-To-Glow™ Dual Secreted Reporter Assay system (Clontech) according to the manufacturers instructions 24h post TNFα treatment.

Cell culture

MDA-MB-231, SUM149PT, MDA-MB-436, MDA-MB-468 triple-negative basal breast cancer cell lines were obtained from ATCC (Manassas, VA) and authenticated before experimental work began by single tandem repeat analysis at 15 different gene loci and amelogenin (Genetica, Burlington, NC). Cell line authentication was performed by Dr. Gray and colleagues. Information about cell culture conditions as well as the source, authentication, clinical, and pathological features of tumors used to derive the breast cancer cell lines used in this study was described in detail previously (8).

siRNA treatment and Synchronization

The cells were transfected with 50nM specified siRNA pools or non-coding control, according to the manufacturer's instructions using RNAiMax (Invitrogen) transfection reagent. Four hours post-transfection, the medium was replaced to the one containing 0.4mM mimosine for 16h. Cells were released from blocking and allowed to progress through the cell cycle for 12h, after which cells were re-blocked with mimosine for 12h. Cells were collected at 10h post-mimosine release for cell cycle analysis. Cell lysates for RNA and protein extraction were collected at 0, and 10h post release from mimosine block.

Cell cycle, apoptosis analysis, and immunoblots

Cell cycle and apoptosis analysis were performed by fluorescence-activated cell sorting (FACS) as well as standard immune blots were generated as described before (3).

Real-Time Quantitative RT-PCR

Total RNA was extracted from cells at 24h and 72h post-siRNA transfection using RNeasy Micro kit (Qiagen). It was reverse-transcribed to cDNA and quantitative RT-PCR analysis using the Taqman assay (ABI) was performed at Genome Analysis Core Facility of Helen Diller Family Comprehensive Cancer Center, UCSF. PCR primers and TaqMan probes for CCND1, TRIB1, IER2, CDKN2C, NUAK1, C14ORF133, CCNE2, TBK1, EGR1, NPC1, SPRED2, KIAA0649, DR5, and YY1 were purchased from Applied Biosystems. hGUS was used as a normalization control. The details of QPCR are described in Supplementary methods.

Transcriptional assessment of MEK inhibition

We assessed the temporal changes in gene expression profiles induced by EGF and UO126 in the MDAMB231 cell line by RNA expression array technology as described in Supplementary Methods.

TaqMan Low density Array (TLDA)

Quantitative PCRs were performed using custom-made TLDA focused on 42 cell cycle related genes (Applied Biosystems; Supplementary Table 3). Normalization of cDNA levels in the different wells was done using the GAPDH and hGUS RNA as a reference. The amplification protocol and data analysis were carried out as previously described (9). Initial data analysis was performed using Qbase-plus software from Biogazelle (http://www.biogazelle.com/). Each sample set was analyzed using the standardization procedure described previously (10).

Microarray RNA expression analaysis

Cell line and treatment preparation—24 hours prior to treatment, cells were transferred to low serum conditions (0.1% FBS), then they were subjected to the following course of treatment. First, we pre-treated the cells with U0126 (10μM) or DMSO (vehicle control) for 30 minutes (time –0.5h). At time 0h, the cells were stimulated with EGF (10ng/ml). Cells were harvested at 8 timepoints: 0, 0.5, 1, 4, 8, 12, 24 and 48h after EGF stimulation (two biological replicates). Total RNA was extracted using the RNeasy Mini kit (Qiagen). Microarray data were generated at the LBNL Molecular Profiling Laboratory using a high-throughput, automated GeneChip® HT System (Affymetrix). HT_HG-U133A array plates consisting of 96 arrays were used. An Affymetrix liquid handling system (GCAS) was used to process the one-cycle IVT target preparation, array plate hybridization setup, washing and staining. Plate scanning was performed using a CCD-based high-throughput scanner (Affymetrix). Expression data have been deposited in the NIH Gene Expression Omnibus (http://www.ncbi.nlm.nih.gov/geo/); accession number: GSE61364.

Processing of microarray data, gene selection, and data frame construction

The quality of the microarray data was assessed using the Simpleaffy package from R/Bioconductor. Microarray data were then normalized using the Robust Multi-array (RMA) method. A subset of genes was then selected to construct the gene regulatory network based on analysis of covariance model to evaluate the significance of each gene in explaining cell cycle progression. The 149 top-ranked genes were identified for inclusion. This list was further supplemented by 20 known cell cycle genes, whose expression was inhibited by treatment with U0126. To learn relationships between drug treatment, mRNA expression profiles, and cell cycle distribution, gene expression measurements at 0, 0.5, and 24 hours were matched with cell cycle distribution data at 0, 24 and 48 hours post-treatment.

Learning an ensemble of probabilistic models from data

An ensemble of Bayesian network models including drug treatment, gene expression and end-point readouts was learned from the data. Bayesian networks provide a convenient framework to represent the global joint probability distribution of $P(X_1 \ldots \ldots X_n : Q)$, where $X_1, \ldots X_n$ are variables in the model and Θ are parameters. As described previously (11), the first phase of learning proceeds by considering all possible combinations of drug, transcripts, and phenotypic data to obtain a collection of highly likely network fragments. Network fragments representing quantitative relationships among all possible sets of two and three measured variables were considered. Each fragment was assigned a Bayesian probabilistic score indicative of how likely the given fragment was given the data, penalized for its mathematical complexity. Here the Laplace approximation (11) was used to integrate over posterior parameter distributions to compute the Bayesian scores for each fragment. In the second phase of learning (6), the network fragments were combined to form an ensemble of models. An ensemble is defined as a statistical sample from the distribution P (Model|Data), the probability distribution over all models given the observed data. A network's score was computed as the sum over the scores of all network component fragments. A parallel global optimization procedure employing simulated annealing (the Metropolis-Hastings algorithm) was used to construct an ensemble of 1024 networks that correctly sampled the probability distribution given the data (6,12).

Model interventional simulations and statistical analysis

Stochastic simulations of the models were used to generate predictions on the distribution of a variable under different conditions (11). Simulations were performed on the ensembles to predict the distribution of model variables under different perturbations. Then the predicted distribution of networks in response to the perturbation was compared to the predicted distribution under baseline expression level of the perturbed transcript. A Student's t-test was used to compute the significance of a transcript's influence on the phenotype and the transcripts were ranked by their p-values.

Identification of drivers of cell cycle progression

To identify genes that were drivers of cell cycle progression, a systematic perturbation procedure was employed. Genes in the model were set to baseline as well as 10 fold below baseline, and cell cycle distribution (%G1) was predicted. All genes were evaluated with this

procedure and the significance of each gene was evaluated via a Student's t-test. The genes were then ranked based on their p-values, which correspond to their likeliness to be causal drivers of cell cycle progression. The p-value was derived based on 30 random samples from the posterior distribution under each simulation condition.

Gene expression, copy number, and survival analysis of primary tumors

In order to evaluate the association between TRIB1 related signaling and clinical characteristics, we exploited a large, clinically annotated breast cancer cohort for which paired Illumina HT-12 expression data and Affymetrix SNP 6.0 copy number data were available (13). Here we report on a subset of 1980 cases to evaluate the correlation between TRIB1 and NFκB/TRAIL signaling as well as clinical outcome associations. In particular, we computed the Pearson correlation between a panel of 38 genes highlighted by functional analyses of breast cancer cell lines and Bayesian network analysis, and reported to be associated with NFκB/TRAIL signaling. Details of this analysis are provided in Supplementary Methods.

Results

A Bayesian network inference model identifies genes involved in G1 arrest in response to MEK inhibition

To assess effects of MEK inhibition on global gene expression profiles and cell cycle distribution, we treated MDA-MB-231 breast cancer cells with U0126, a small-molecule inhibitor of MEK1/2, (Fig. S1). To infer relationships between drug treatment, mRNA expression profiles, and cell cycle distribution, gene expression measurements at 0, 0.5, and 24 hours were matched with cell cycle distribution data at 0, 24 and 48 hours post-treatment. Initial statistical analysis of the data identified 149 genes that were significantly correlated with cell cycle arrest following drug treatment (Table S1). An additional 20 known cell cycle genes, whose expression levels were significantly changed by U0126, were also included in the analysis (Table S1). These data were used to reverse-engineer an ensemble of 1024 Bayesian networks (Fig. 1). The inclusion of the 20 known cell cycle genes impacted by U0126 served as a positive control for testing the models as we expected the model predictions to recover some of the known biology. The ensemble of networks was reverse-engineered from the data in two steps (6,7,14,15). First, a Bayesian score, which takes into account the uncertainty in the parameters and penalizes for complexity, was computed for all possible two and three-element sub-networks. Second, Metropolis Monte Carlo global optimization was used to infer a statistical sample, or ensemble, of network structures from these sub-networks that was consistent with the data (6). Variance in the ensemble reflected uncertainty in network structure given the information available in the data (6). In this analysis we retained both the network topology structures as well as the parameterization of the sub-networks in order to generate quantitative predictions on the effect of gene interventions that account for uncertainty in network topologies (6). Next, systematic *in silico* simulations of 10-fold knockdown of each of the 169 transcripts were completed to predict their effect on G1-S transition. This was accomplished by setting the value of a gene expression variable to 10% of its original value, and then propagating the effects of the intervention through the network structure, and generating out-of-sample simulated values

for the G1 fraction under the knockdown condition (Fig. S2). Since all networks in the ensemble of models are likely given the data, the entire distribution of predictions generated from the ensemble of networks was analyzed for statistical differences between the knockdown and no-knockdown simulation conditions using a paired t-test that samples from the distribution 30 times.

Using this approach, we identified 12 genes as candidate regulators of G1-S transition, based on a significance level of p<0.01 (Table S1). These genes included known regulators of G1-S transition (*CCND1* (16,17), *CCNE2* (18), *CDC25A* (19), *CDKN2C* (20), *NUAK*1 (21)) as well as novel candidates (*TRIB1, IER2, C14ORF133, TAF11, EBAG9, COQ9*, and *TRIM27*).

Experimental validation of model predictions

To validate the model predictions, we assessed cell cycle distribution in cells treated with pools of short-interfering RNAs (siRNA) (Fig. 2a). We utilized pools of siRNA since they have been demonstrated to result in greater phenotypic penetrance and reduced off-target effects compared to single siRNAs (22). Cells were treated with pools of siRNAs directed against the 12 candidate genes and 5 genes (*NPC1, EGR1, SPRED2, BTG3, KIAA0649*) that were predicted to have no effect on G1-S phase transition as negative controls, as well as non-coding control siRNAs (Table S2). Target knock-down was confirmed by mRNA analysis and protein levels (where antibodies were available) (Fig. S3). Fluorescence-activated cell sorting (FACS) analysis of cell cycle distribution confirmed the established role of CCND1, CDC25a, and CCNE2 in G1 to S progression, and validated model predictions for novel candidate regulators such as IER2, TRIB1*,* NUAK1, C14ORF133, TRIM27, TAF11, and EBAG9 (Fig. 2a). However, we saw no effect on G1-S transition with siRNAs directed against CDKN2C and COQ9, while knockdown of KIAA0649, a negative control, resulted in G1 arrest. Effect of individual siRNA duplexes against TRIB1 on cell cycle was also analyzed (Fig. S4). Overall, the model predicted the effect of interventions with 82% accuracy, 91% sensitivity, and 67% specificity. To understand the mechanism of G1 arrest, we analyzed the status of proteins known to promote G1-S transition (CCND1, CCNA2, CCNE2, phospho-CDK2, ppRB), as well as inhibitors (p27, p18) (Fig. 2b,c). We found that knock down of genes leading to G1 arrest resulted in at least a 2-fold increase in protein levels of p27, p18 or both, with the exception of TRIM27 and KIAA0649. Simultaneously, knock down of these genes resulted in inhibition of at least three promoters of G1-S transition (Fig. 2c). Analysis of mRNA expression of 46 genes associated with G1-S progression showed distinct patterns of gene expression after siRNA treatment that confirmed the protein findings for CCND1, CCNA2, and CCNE2 (Fig. S5).

TRIB1 regulates CCND1 expression via kappaB and AP1 sites

TRIB1 was predicted by the model to regulate G1-S phase transition with the highest significance score (p=$2.49E^{-10}$). Its siRNA-mediated knockdown resulted in inhibition of cyclin D1 RNA and protein levels (Fig. 2b, Fig. S5). To investigate the mechanism of TRIB1 knockdown effect on CCND1 expression we evaluated its effect on the activity of CCND1 promoter using constructs containing mutations in AP1, NFκB, and Ets transcription factor-binding sites (Fig. 3a–b). In cells treated with NC siRNA, inactivation of either both NFκB

(D1-κB1/2M) sites or AP1 site led to inhibition of CCND1 promoter activity, while inactivation of the two Ets sites had no effect. TRIB1 knockdown resulted in 2-fold downregulation of wild type CCND1 (D1-WT) promoter activity with further reduction in activity of D1-κB1/2M and AP1 promoter constructs, indicating that TRIB1 signals upstream of both ERK1/2 and NFκB (Fig. 3b).

TRIB1 mediates NFkB-responsive promoter activity and expression of CXCL1, CSF2, and IL8

To confirm the role of TRIB1 in regulation of NFκB activity we analyzed the effect of TRIB1 knockdown and overexpression on an NFκB-responsive promoter construct. This analysis showed that TRIB1 knockdown inhibited the activity of an NFκB-responsive promoter, while TRIB1 overexpression led to a 3-fold increase in promoter activity (Fig. 3c, Fig. S6). The expression of siRNA-resistant TRIB1 rescued the phenotype induced by siRNA-mediated TRIB1 knockdown (Fig. S7). Furthermore, evaluation of the expression of NFκB target genes involved in metastasis formation (CSF2, CXCL1) and tumor inflammation (IL8) showed that inhibition of TRIB1 with siRNA resulted in downregulation of these genes on RNA and protein levels (Fig. 3d, Fig. S8). Activation of NFκB is mediated by inactivation of its inhibitors IκBα, p100 and p105 (23) by several upstream kinases, including IKKα. We reasoned that TRIB1 may act upstream of NFκB. TRIB1 knockdown inhibited phosphorylation and degradation of IκBα as well as production of p50 from its precursor p105 (Fig. 3e, Fig. S9). Additionally, we found that phosphorylation of IKKα/β (Ser176/180), of IKKα (Thr 23) as well as expression of p100 and its processing with generation of p52 were significantly inhibited by downregulation of TRIB1, possibly indicating regulation of p100 expression by TRIB1 (Fig. 3e, Fig S9). These findings provide mechanistic evidence for regulation of NFκB by TRIB1. No changes in RalA phosphorylation at serine 536 were observed. While IKKα and AKT have been shown to phosphorylate RelA, multiple additional kinases are known to phosphorylate RelA at the same site and might maintain phosphorylation following knock-down of TRIB1 (24,25).

TRIB1 regulates activity of the PI3K-AKT pathway

One of the potential mechanisms of the cytostatic rather then cytotoxic effect of MEK inhibition is activation of a feedback loop leading to upregulation of AKT signaling (3). In contrast, TRIB1 knockdown leads to simultaneous inhibition of phosphorylation of ERK1/2 and AKT1 on both T308 and S473 (Fig. 4a). Assessment of downstream targets of AKT kinase revealed that TRIB1 knockdown led to inhibition of phosphorylation of BCL2, GSK3α/β, and FOXO1A/3A (Fig. 4a). Additionally, we observed inhibition of phosphorylation of IKKα-T23, an AKT-specific site, providing further evidence for a putative mechanism of NFκB regulation by TRIB1 through its role as a mediator of PI3-kinase-AKT signaling (Fig. 3e).

TRIB1 inhibition upregulates DR5 levels and sensitizes breast cancer cells to TRAIL-induced apoptosis

We postulated that inhibition of anti-apoptotic and induction of pro-apoptotic signals results in increased cell death upon TRIB1 knockdown alone or in combination with the death receptor agonist TRAIL. Treatment of cells with TRIB1 siRNA alone resulted in an increase

in apoptosis in all cell lines tested (Fig. 4b). We also observed a 2–3 fold increase in apoptosis in cells treated with TRIB1 siRNA in combination with TRAIL treatment (Fig. 4c). These observations were in accord with the induction of PARP cleavage (Fig. 4d). TRAIL-induced apoptosis occurs through an extrinsic mechanism of direct activation of executioner caspases by receptor-activated caspase-8 (26). In addition, apoptosis can be amplified via recruitment of the intrinsic mitochondrial pathway. Activated caspase-8 cleaves pro-apoptotic protein BID, leading to its translocation to the mitochondria and resulting in mitochondrial apoptosis activation (26). TRIB1 knockdown resulted in increased caspase-8 cleavage (Fig. S10), as well as decreased levels of FLIP and BID, indicating increased cleavage of these proteins and the involvement of both pathways (Fig. 4d). To explain how TRIB1 inhibition leads to up-regulation of TRAIL-induced apoptosis we assayed both mRNA and protein levels of TRAIL Receptor 2 (DR5). DR5 expression is negatively regulated by NFκB via induction of the transcriptional inhibitor YY1 (27). Here we show that knockdown of TRIB1 leads to significant upregulation of both, DR5 mRNA and protein levels, as well as downregulation of YY1 mRNA (Fig. 4e,f; Fig. S11). These data suggest that TRIB1 knockdown sensitizes cells to TRAIL-induced apoptosis by inhibition of NFκB signaling and upregulation of DR5, as well as by inhibition of AKT pro-survival signaling.

Association between TRIB1/TRAIL/NFkB signaling components in human breast cancer

To establish the significance of TRIB1/TRAIL/NFkB signaling in the context of human disease and to perform exploratory tests of clinical outcome associations, we exploited a large cohort (n=1980) of primary breast tumors, with long-term clinical follow-up and which have been profiled at the genomic and transcriptomic levels (13). Given our finding that TRIB1 mediates cyclin D1 expression via the regulation of NFκB and AP1, with TRIB1 knockdown resulting in the downregulation of NFκB targets *in vitro*, we first sought to examine these relationships in the human system. In agreement with our earlier findings, *TRIB1* and *NFKB1*(p105) expression levels were significantly correlated (ρ=0.102, p<0.0001), and *TRIB1* was correlated with the expression of the NFκB target genes *IL8* (ρ=0.05, p<0.05) and *CSF2* (ρ=0.05, p<0.005). We also comprehensively examined the relationships between TRIB1, TRAIL, and NFκB signaling using this tumor cohort to compare the correlations between a panel of 38 genes believed to be associated with these pathways based on the literature (Fig. 5a). In addition to those listed above, we found that the following gene sets were significantly (p<0.05) positively correlated with *TRIB1*: proliferation associated genes (*CCND1, TOP2A, MCM2, MKI67*), the anti-apoptotic genes (*BCL2L1, BCL2L11, CFLAR*), the pro-apoptotic genes (*BIK, HRK*), components of the death receptor complex (*TRAF2, TRAF6),* as well as *TNFRSF10A/DR4* and *IL6*. A small number of genes in each of these categories were negatively correlated with *TRIB1*, including *PCNA* (proliferation), *BCL2LA1* (anti-apoptotic) and *BAD* (pro-apoptotic)*, TRADD* and *MPRIP* (death receptor complex), and *CASP3* (caspase activity) (Fig. 5a). These findings are in agreement with our observation that TRIB1 knockdown sensitizes cells to TRAIL-induced apoptosis, resulting in increased cleavage of both BID and CFLAR in breast cancer cells and supports the role of TRIB1 in cell cycle progression and survival.

Association between TRIB1/TRAIL/NFκB associated gene expression profiles and TRIB1 copy number with clinical outcome

We next sought to explore the correlation between TRIB1/TRAIL/NFkB associated genes and patient survival in a human breast tumor cohort. A comparison of Kaplan-Meier curves for TRIB1 copy number amplified versus neutral cases suggests an association with both breast cancer specific (BCSS) (log-rank p-value <0.01) and overall survival (OS) (log-rank p-value <0.01) (Fig. 5b, Table S4). In order to visualize the association between TRIB1 or other single gene expression models and outcome in an exploratory analysis, continuous expression levels were stratified into tertiles, and the predicted survival curves for individuals in the upper (66.66%) and lower (33.33%) groups were compared using Kaplan-Meier plots and the log-rank test. These comparisons suggest an association between both *TRIB1* and *IL8* expression and outcome, as assessed by both BCSS (log-rank p-value <0.01) and OS (log-rank p-value <0.05) (Fig. S12a–d).

To investigate these relationships further, while adjusting for clinically relevant covariates, we examined survival as a function of continuous gene expression data for single and multiple gene models based on the panel of 38 TRIB1/TRAIL/NFkB associated genes using Cox regression. In particular, multivariable analysis was performed by building Cox proportional hazards models, which included the most relevant clinical variables as covariates, namely, age, number of lymph nodes positive, tumor size, and grade, stratified by ER status and tumor bank in order to test for differences in BCSS and OS associated with these genes, as described in the Methods section. After adjusting for these variables, only *BIK, MPRIP, IL8*, and *TOP2A* were significant (Wald test, p<0.05) in the full cohort, where BCSS was the outcome (Fig. S13, Table S5). For OS *BIK, MPRIP,* and *TOP2A* were again significant, as were *HRK* and *CASP3,* whereas *IL8* was not associated with this outcome (Fig. S14, Table S6).

Discussion

MEK-dependent signaling is a highly complex process as highlighted by our previously described finding of an EGFR-dependent feedback loop resulting in activation of the PI3 kinase pathway following MEK inhibition (3). Studies broadly assessing protein expression changes following MEK inhibitor treatment corroborate these findings (28). Among the best-documented cellular consequences of MEK inhibition is induction of cell cycle arrest, predominantly at the G1-S phase transition (3,29,30). This cytostatic effect is mediated by a variety of mechanisms (reviewed in (31)) including repression of cyclin D1 (32). The work presented here sheds new light onto the intermediary steps downstream of MEK and upstream of CCND1. We utilized an advanced Bayesian network inference engine to deepen our understanding of molecular networks driving responses of cancer cells to MEK inhibition.

Bayesian network inference models allow for reconstruction of molecular networks and for making causal predictions about the relationships of individual network components. While the Bayesian approach has been applied to the reconstruction of small signal transduction networks before (33,34), our study involves automated construction of large ensembles of networks and extensive experimental validation. Our model predictions correctly identify the

established role of CCND1, CCNE2, CDC25a, and ARK5/NUAK1 in regulation of G1-S progression. Moreover, we identified and experimentally validated TRIB1, IER2, C14ORF133, TAF11, EBAG9, and TRIM27 as novel regulators of G1-S transition. The high rate of validated predictions underscores the power of simulatable Bayesian models.

In the model, TRIB1 was the highest ranked gene (p-val=$2.49E^{-10}$) in our list of genes predicted to affect cell cycle distribution. During *Drosophila* development, *Tribbles* has been demonstrated to regulate G2-M transition during *anlage* formation through a cdc25-dependent mechanism (35,36). TRIB1 has recently been shown to control differentiation of M2-like macrophages in C/EBPα-dependent manner (37) and it has been implicated in proliferation and chemotaxis of vascular smooth muscle cells via regulation of MAPK activity (38). Most importantly in the context of the current study, TRIB1 and TRIB2 have been demonstrated to be sufficient to induce leukemia in mice when overexpressed (39). However, the role of TRIB1 in regulation of the mammalian cell cycle remains unknown. In this study, we present evidence that TRIB1 is involved in regulation of G1-S progression by modulating CCND1 expression in human breast cancer cells. CCND1 is highly overexpressed and a pivotal driver of G1-S progression in these cells (40). The CCND1 promoter contains binding sites for multiple transcription factors including four Ets, two NFκB, and one AP1 site (41–43). We found that TRIB1 regulates NFκB and AP1-dependent transactivation of the CCND1 gene. These findings support our observation that TRIB1 knockdown leads to downregulation of CCND1 protein and RNA levels. Indeed, TRIB1 was found to act upstream of the MAPKK SEK1 in C. elegance (44) and it has been shown to physically interact with MEK1 and p65 subunit of NFκB in mammalian cells and to promote induction of pro-inflammatory cytokines in lipocytes (45). Moreover, NFκB has been demonstrated to enhance AP-1 dependent transactivation in lymphocytes (46). Thus, our data illuminate a role for TRIB1 in regulating MAPK-dependent signals, and, in a broader sense, in oncogenesis and inflammation. Interestingly, our data demonstrate that TRIB1 RNA expression might be regulated through the MAPK pathway, suggesting a feed-forward mechanism by which signals through the MAPK pathway increase TRIB1 expression which, in turn, further stimulates signaling through the pathway. This possibility is subject of ongoing investigation. Other TRIB-family members, in particular TRIB3, have been shown to interact with MAPK and Notch signaling in breast cancer, highlight these pseudo-kinases as modulators of key oncogenic signaling pathways (47).

Recent studies revealed upregulation of TRIB1 during acute and chronic inflammation in white adipose tissue of mice (48). In agreement with these findings, we observed inhibition of CXCL1, CSF2 and IL8 expression in response to treatment with TRIB1 siRNA, as well as upregulation of these genes in cells overexpressing TRIB1 construct. It remains to be determined whether TRIB1 serves as a nuclear co-activator of p65 subunit in mammary epithelial cells. However, we found that knock-down of TRIB1 leads to inhibition of pIKKα, pIκBα, and subsequent pIκBα degradation. These findings point to a cytoplasmic role of TRIB1 in regulation of NFkB-dependent transcription. Phosphorylation of IKKα on Tyrosine-23 has been shown to be strongly dependent on AKT (49). In addition, we observed inhibition of multiple components of the PI3K pathway in response to knock-down of TRIB1, providing evidence that TRIB1 influences signal transduction of the PI3K-NFκB pathways beyond the nucleus. TRIB1 functions, at least in part, as a scaffold protein (50)

suggesting that TRIB1 might mediate protein-protein interactions of key regulators of the PI3K and NFκB pathways resulting in their activation. This possibility is currently under investigation.

Regulation of apoptosis represents one of the main functions of the NFκB pathway. In solid tumors, the pathway predominantly suppresses apoptosis induction through a multitude of mechanisms (reviewed in: (51)) and has been shown to be a major contributor to resistance to chemotherapeutic agents (52). Suppression of death-receptor signaling by NFkB has been implicated as one possible mechanism (53). Our work demonstrates that knock-down of TRIB1 induces death receptor signaling by down-regulation of DR5 transcriptional repressor, YY1, resulting in significant increase of DR5 levels. Regulation of YY1 by NFκB is well-documented (54). Despite promising preclinical results, initial clinical experience with death receptor agonists for solid tumor indications have been disappointing (55). Based on our findings, we speculate that high expression levels of TRIB1 contribute to resistance to this class of drugs and that inhibitors of TRIB1 activity could overcome therapeutic resistance.

Discovery of involvement of TRIB1 in regulating proliferation, apoptosis, and cytokine production suggests that high levels of TRIB1 expression might result in a clinically more aggressive tumor phenotype. In agreement with this hypothesis we found that increased DNA copy numbers of the *TRIB1* gene as well as high level of TRIB1 mRNA expression are associated with poor breast cancer survival in a large cohort of breast cancers (13). TRIB1 is located on chromosome 8q24 in immediate vicinity of the oncogene cMyc, which is often amplified in cancer. Furthermore, we found TRIB1 expression to be associated with elements of the NFκB network (e.g. *NFKB1, IL8*) that we had identified to be down-stream of TRIB1 in our in vitro studies. Based on the association of TRIB1 with a key survival endpoint in breast cancer and its biological functions, we are currently pursuing studies to evaluate its potential as a target for therapeutic intervention.

In summary, our study highlights that linear signal transduction cascades, such as the RAS-RAF-MEK-ERK module, are embedded in complex molecular networks. We show that the combination of Bayesian network inference models, *in silico* simulation, and *in vitro* validation represents a powerful new approach for discerning non-intuitive relationships and generation of testable hypotheses about signaling networks from a large, multi-dimensional data set. By applying this strategy, we identified TRIB1 as an important mediator of key signal transduction pathways and a candidate therapeutic target in breast cancer.

Supplementary Material

Refer to Web version on PubMed Central for supplementary material.

Acknowledgments

References

1. Wang D, Boerner SA, Winkler JD, LoRusso PM. Clinical experience of MEK inhibitors in cancer therapy. Biochim Biophys Acta. 2007; 1773(8):1248–55. S0167-4889(06)00369-7 [pii]. DOI: 10.1016/j.bbamcr.2006.11.009 [PubMed: 17194493]

2. Friday BB, Adjei AA. Advances in targeting the Ras/Raf/MEK/Erk mitogen-activated protein kinase cascade with MEK inhibitors for cancer therapy. Clin Cancer Res. 2008; 14(2):342–6. 14/2/342 [pii]. DOI: 10.1158/1078-0432.CCR-07-4790 [PubMed: 18223206]

3. Mirzoeva OK, Das D, Heiser LM, Bhattacharya S, Siwak D, Gendelman R, et al. Basal subtype and MAPK/ERK kinase (MEK)-phosphoinositide 3-kinase feedback signaling determine susceptibility of breast cancer cells to MEK inhibition. Cancer research. 2009; 69(2):565–72. 69/2/565 [pii]. DOI: 10.1158/0008-5472.CAN-08-3389 [PubMed: 19147570]

4. Turke AB, Song Y, Costa C, Cook R, Arteaga CL, Asara JM, et al. MEK inhibition leads to PI3K/AKT activation by relieving a negative feedback on ERBB receptors. Cancer research. 2012; 72(13):3228–37. 0008-5472.CAN-11-3747 [pii]. DOI: 10.1158/0008-5472.CAN-11-3747 [PubMed: 22552284]

5. Janes KA, Lauffenburger DA. A biological approach to computational models of proteomic networks. Curr Opin Chem Biol. 2006; 10(1):73–80. S1367-5931(05)00168-7 [pii]. DOI: 10.1016/j.cbpa.2005.12.016 [PubMed: 16406679]

6. Xing H, McDonagh PD, Bienkowska J, Cashorali T, Runge K, Miller RE, et al. Causal modeling using network ensemble simulations of genetic and gene expression data predicts genes involved in rheumatoid arthritis. PLoS Comput Biol. 2011; 7(3):e1001105.doi: 10.1371/journal.pcbi.1001105 [PubMed: 21423713]

7. Friedman N, Koller D. Being Bayesian About Network Structure. A Bayesian Approach to Structure Discovery in Bayesian Networks. Machine Learning. 2003; 50(1–2):95–125. DOI: 10.1023/a:1020249912095

8. Neve RM, Chin K, Fridlyand J, Yeh J, Baehner FL, Fevr T, et al. A collection of breast cancer cell lines for the study of functionally distinct cancer subtypes. Cancer cell. 2006; 10(6):515–27. [PubMed: 17157791]

9. Ermonval M, Petit D, Le Duc A, Kellermann O, Gallet PF. Glycosylation-related genes are variably expressed depending on the differentiation state of a bioaminergic neuronal cell line: implication for the cellular prion protein. Glycoconj J. 2009; 26(4):477–93. DOI: 10.1007/s10719-008-9198-5 [PubMed: 18937066]

10. Willems E, Leyns L, Vandesompele J. Standardization of real-time PCR gene expression data from independent biological replicates. Anal Biochem. 2008; 379(1):127–9. S0003-2697(08)00264-9 [pii]. DOI: 10.1016/j.ab.2008.04.036 [PubMed: 18485881]

11. Tierney L, Kadane JB. Accurate approximations for posterior moments and marginal densities. J Ameri Stat Assoc. 1986; 81(393):82–6.

12. Ding Y, Lawrence CE. A statistical sampling algorithm for RNA secondary structure prediction. Nucleic Acids Res. 2003; 31(24):7280–301. [PubMed: 14654704]

13. Curtis C, Shah SP, Chin SF, Turashvili G, Rueda OM, Dunning MJ, et al. The genomic and transcriptomic architecture of 2,000 breast tumours reveals novel subgroups. Nature. 2012; 486(7403):346–52. nature10983 [pii]. DOI: 10.1038/nature10983 [PubMed: 22522925]

14. Friedman N, Linial M, Nachman I, Pe'er D. Using Bayesian networks to analyze expression data. J Comput Biol. 2000; 7(3–4):601–20. [PubMed: 11108481]

15. Sachs K, Perez O, Pe'er D, Lauffenburger DA, Nolan GP. Causal protein-signaling networks derived from multiparameter single-cell data. Science (New York, NY. 2005; 308(5721):523–9. 308/5721/523 [pii]. DOI: 10.1126/science.1105809

16. Baldin V, Lukas J, Marcote MJ, Pagano M, Draetta G. Cyclin D1 is a nuclear protein required for cell cycle progression in G1. Genes Dev. 1993; 7(5):812–21. [PubMed: 8491378]

17. Stacey DW. Cyclin D1 serves as a cell cycle regulatory switch in actively proliferating cells. Curr Opin Cell Biol. 2003; 15(2):158–63. d[pii]. [PubMed: 12648671]

18. Aleem E, Kiyokawa H, Kaldis P. Cdc2-cyclin E complexes regulate the G1/S phase transition. Nature cell biology. 2005; 7(8):831–6. ncb1284 [pii]. DOI: 10.1038/ncb1284 [PubMed: 16007079]

19. Jinno S, Suto K, Nagata A, Igarashi M, Kanaoka Y, Nojima H, et al. Cdc25A is a novel phosphatase functioning early in the cell cycle. EMBO J. 1994; 13(7):1549–56. [PubMed: 8156993]

20. Latres E, Malumbres M, Sotillo R, Martin J, Ortega S, Martin-Caballero J, et al. Limited overlapping roles of P15(INK4b) and P18(INK4c) cell cycle inhibitors in proliferation and tumorigenesis. EMBO J. 2000; 19(13):3496–506. DOI: 10.1093/emboj/19.13.3496 [PubMed: 10880462]

21. Humbert N, Navaratnam N, Augert A, Da Costa M, Martien S, Wang J, et al. Regulation of ploidy and senescence by the AMPK-related kinase NUAK1. EMBO J. 2010; 29(2):376–86. emboj2009342 [pii]. DOI: 10.1038/emboj.2009.342 [PubMed: 19927127]

22. Parsons BD, Schindler A, Evans DH, Foley E. A direct phenotypic comparison of siRNA pools and multiple individual duplexes in a functional assay. PLoS One. 2009; 4(12):e8471.doi: 10.1371/journal.pone.0008471 [PubMed: 20041186]

23. Oeckinghaus A, Ghosh S. The NF-kappaB family of transcription factors and its regulation. Cold Spring Harb Perspect Biol. 2009; 1(4):a000034.doi: 10.1101/cshperspect.a000034 [PubMed: 20066092]

24. Bohuslav J, Chen LF, Kwon H, Mu Y, Greene WC. p53 induces NF-kappaB activation by an IkappaB kinase-independent mechanism involving phosphorylation of p65 by ribosomal S6 kinase 1. The Journal of biological chemistry. 2004; 279(25):26115–25. DOI: 10.1074/jbc.M313509200 [PubMed: 15073170]

25. Ghosh S, Karin M. Missing pieces in the NF-kappaB puzzle. Cell. 2002; 109(Suppl):S81–96. [PubMed: 11983155]

26. Johnstone RW, Frew AJ, Smyth MJ. The TRAIL apoptotic pathway in cancer onset, progression and therapy. Nat Rev Cancer. 2008; 8(10):782–98. nrc2465 [pii]. DOI: 10.1038/nrc2465 [PubMed: 18813321]

27. Martinez-Paniagua MA, Baritaki S, Huerta-Yepez S, Ortiz-Navarrete VF, Gonzalez-Bonilla C, Bonavida B, et al. Mcl-1 and YY1 inhibition and induction of DR5 by the BH3-mimetic Obatoclax (GX15-070) contribute in the sensitization of B-NHL cells to TRAIL apoptosis. Cell Cycle. 2011; 10(16):2792–805. [pii]. [PubMed: 21822052]

28. Duncan JS, Whittle MC, Nakamura K, Abell AN, Midland AA, Zawistowski JS, et al. Dynamic reprogramming of the kinome in response to targeted MEK inhibition in triple-negative breast cancer. Cell. 2012; 149(2):307–21. S0092-8674(12)00350-9 [pii]. DOI: 10.1016/j.cell.2012.02.053 [PubMed: 22500798]

29. Gysin S, Lee SH, Dean NM, McMahon M. Pharmacologic inhibition of RAF-->MEK-->ERK signaling elicits pancreatic cancer cell cycle arrest through induced expression of p27Kip1. Cancer research. 2005; 65(11):4870–80. 65/11/4870 [pii]. DOI: 10.1158/0008-5472.CAN-04-2848 [PubMed: 15930308]

30. Sebolt-Leopold JS, Dudley DT, Herrera R, Van Becelaere K, Wiland A, Gowan RC, et al. Blockade of the MAP kinase pathway suppresses growth of colon tumors in vivo. Nat Med. 1999; 5(7):810–6. [PubMed: 10395327]

31. Chambard JC, Lefloch R, Pouyssegur J, Lenormand P. ERK implication in cell cycle regulation. Biochim Biophys Acta. 2007; 1773(8):1299–310. S0167-4889(06)00379-X [pii]. DOI: 10.1016/j.bbamcr.2006.11.010 [PubMed: 17188374]

32. Weber JD, Raben DM, Phillips PJ, Baldassare JJ. Sustained activation of extracellular-signal-regulated kinase 1 (ERK1) is required for the continued expression of cyclin D1 in G1 phase. The Biochemical journal. 1997; 326(Pt 1):61–8. [PubMed: 9337851]

33. Hill SM, Lu Y, Molina J, Heiser LM, Spellman PT, Speed TP, et al. Bayesian inference of signaling network topology in a cancer cell line. Bioinformatics (Oxford, England). 2012; 28(21):2804–10. bts514 [pii]. DOI: 10.1093/bioinformatics/bts514

34. Froehlich H, Fellmann M, Sueltmann H, Poustka A, Beissbarth T. Large scale statistical inference of signaling pathways from RNAi and microarray data. BMC Bioinformatics. 2007; 8:386. 1471-2105-8-386 [pii]. doi: 10.1186/1471-2105-8-386 [PubMed: 17937790]

35. Seher TC, Leptin M. Tribbles, a cell-cycle brake that coordinates proliferation and morphogenesis during Drosophila gastrulation. Curr Biol. 2000; 10(11):623–9. [pii]. [PubMed: 10837248]

36. Mata J, Curado S, Ephrussi A, Rorth P. Tribbles coordinates mitosis and morphogenesis in Drosophila by regulating string/CDC25 proteolysis. Cell. 2000; 101(5):511–22. [pii]. [PubMed: 10850493]

37. Satoh T, Kidoya H, Naito H, Yamamoto M, Takemura N, Nakagawa K, et al. Critical role of Trib1 in differentiation of tissue-resident M2-like macrophages. Nature. 2013; 495(7442):524–8. nature11930 [pii]. DOI: 10.1038/nature11930 [PubMed: 23515163]

38. Sung HY, Guan H, Czibula A, King AR, Eder K, Heath E, et al. Human tribbles-1 controls proliferation and chemotaxis of smooth muscle cells via MAPK signaling pathways. The Journal of biological chemistry. 2007; 282(25):18379–87. M610792200 [pii]. DOI: 10.1074/jbc.M610792200 [PubMed: 17452330]

39. Dedhia PH, Keeshan K, Uljon S, Xu L, Vega ME, Shestova O, et al. Differential ability of Tribbles family members to promote degradation of C/EBPalpha and induce acute myelogenous leukemia. Blood. 2010; 116(8):1321–8. DOI: 10.1182/blood-2009-07-229450 [PubMed: 20410507]

40. Hosokawa Y, Arnold A. Mechanism of cyclin D1 (CCND1, PRAD1) overexpression in human cancer cells: analysis of allele-specific expression. Genes Chromosomes Cancer. 1998; 22(1):66–71. [pii]. DOI: 10.1002/(SICI)1098-2264(199805)22:1<66::AID-GCC9>3.0.CO;2-5 [PubMed: 9591636]

41. Tetsu O, McCormick F. Beta-catenin regulates expression of cyclin D1 in colon carcinoma cells. Nature. 1999; 398(6726):422–6. [PubMed: 10201372]

42. Hinz M, Krappmann D, Eichten A, Heder A, Scheidereit C, Strauss M. NF-kappaB function in growth control: regulation of cyclin D1 expression and G0/G1-to-S-phase transition. Mol Cell Biol. 1999; 19(4):2690–8. [PubMed: 10082535]

43. Klein EA, Assoian RK. Transcriptional regulation of the cyclin D1 gene at a glance. J Cell Sci. 2008; 121(Pt 23):3853–7. DOI: 10.1242/jcs.039131 [PubMed: 19020303]

44. Pujol N, Cypowyj S, Ziegler K, Millet A, Astrain A, Goncharov A, et al. Distinct innate immune responses to infection and wounding in the C. elegans epidermis. Curr Biol. 2008; 18(7):481–9. S0960-9822(08)00361-8 [pii]. DOI: 10.1016/j.cub.2008.02.079 [PubMed: 18394898]

45. Kiss-Toth E, Bagstaff SM, Sung HY, Jozsa V, Dempsey C, Caunt JC, et al. Human tribbles, a protein family controlling mitogen-activated protein kinase cascades. The Journal of biological chemistry. 2004; 279(41):42703–8. M407732200 [pii]. DOI: 10.1074/jbc.M407732200 [PubMed: 15299019]

46. Krappmann D, Wegener E, Sunami Y, Esen M, Thiel A, Mordmuller B, et al. The IkappaB kinase complex and NF-kappaB act as master regulators of lipopolysaccharide-induced gene expression and control subordinate activation of AP-1. Mol Cell Biol. 2004; 24(14):6488–500. 24/14/6488 [pii]. DOI: 10.1128/MCB.24.14.6488-6500.2004 [PubMed: 15226448]

47. Izrailit J, Berman HK, Datti A, Wrana JL, Reedijk M. High throughput kinase inhibitor screens reveal TRB3 and MAPK-ERK/TGFbeta pathways as fundamental Notch regulators in breast cancer. Proceedings of the National Academy of Sciences of the United States of America. 2013; 110(5):1714–9. DOI: 10.1073/pnas.1214014110 [PubMed: 23319603]

48. Ostertag A, Jones A, Rose AJ, Liebert M, Kleinsorg S, Reimann A, et al. Control of adipose tissue inflammation through TRB1. Diabetes. 2010; 59(8):1991–2000. db09-1537 [pii]. DOI: 10.2337/db09-1537 [PubMed: 20522600]

49. Ozes ON, Mayo LD, Gustin JA, Pfeffer SR, Pfeffer LM, Donner DB. NF-kappaB activation by tumour necrosis factor requires the Akt serine-threonine kinase. Nature. 1999; 401(6748):82–5. DOI: 10.1038/43466 [PubMed: 10485710]

50. Sung HY, Francis SE, Crossman DC, Kiss-Toth E. Regulation of expression and signalling modulator function of mammalian tribbles is cell-type specific. Immunol Lett. 2006; 104(1–2):171–7. DOI: 10.1016/j.imlet.2005.11.010 [PubMed: 16364454]

51. Prasad S, Ravindran J, Aggarwal BB. NF-kappaB and cancer: how intimate is this relationship. Mol Cell Biochem. 2010; 336(1–2):25–37. DOI: 10.1007/s11010-009-0267-2 [PubMed: 19823771]

52. Li F, Sethi G. Targeting transcription factor NF-kappaB to overcome chemoresistance and radioresistance in cancer therapy. Biochim Biophys Acta. 2010; 1805(2):167–80. S0304-419X(10)00003-X [pii]. DOI: 10.1016/j.bbcan.2010.01.002 [PubMed: 20079806]

53. Debatin KM, Krammer PH. Death receptors in chemotherapy and cancer. Oncogene. 2004; 23(16): 2950–66. 1207558 [pii]. DOI: 10.1038/sj.onc.1207558 [PubMed: 15077156]

54. Baritaki S, Huerta-Yepez S, Sakai T, Spandidos DA, Bonavida B. Chemotherapeutic drugs sensitize cancer cells to TRAIL-mediated apoptosis: up-regulation of DR5 and inhibition of Yin Yang 1. Molecular cancer therapeutics. 2007; 6(4):1387–99. 6/4/1387 [pii]. DOI: 10.1158/1535-7163.MCT-06-0521 [PubMed: 17431117]

55. Dimberg LY, Anderson CK, Camidge R, Behbakht K, Thorburn A, Ford HL. On the TRAIL to successful cancer therapy? Predicting and counteracting resistance against TRAIL-based therapeutics. Oncogene. 2013; 32(11):1341–50. onc2012164 [pii]. DOI: 10.1038/onc.2012.164 [PubMed: 22580613]
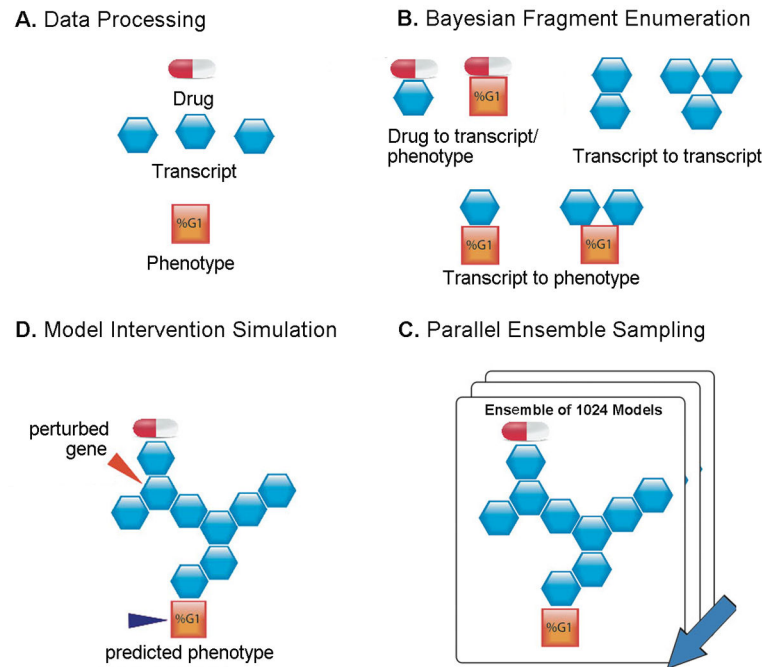
Figure 1. Schematic of Bayesian network Reverse-Engineering and Forward-Simulation
**A**. Drug treatment (as an icon of drug pill), gene expression (blue hexagon) and phenotypic data (orange square) are prepared for modeling via procedures outlined in the supplementary section. **B.** Likely fragments for network reconstruction were identified by scoring all 2- and 3-variable combinations with the constraint that drug treatment is upstream of all other nodes. **C.** Parallel global network sampling results in an ensemble of 1024 network structures that explain the data. The probabilistic directionality computed by the Bayesian framework allows inferences to be made about what lies upstream and downstream of a particular variable of interest. **D.** Diversity of network structures captures uncertainty in the model. Hypotheses can be extracted from the network ensemble by completing Monte Carlo simulations of "what-if" scenarios. Down-regulating a transcript indicated by red arrow would be expected to impact the phenotype (the orange square next to dark blue arrow).
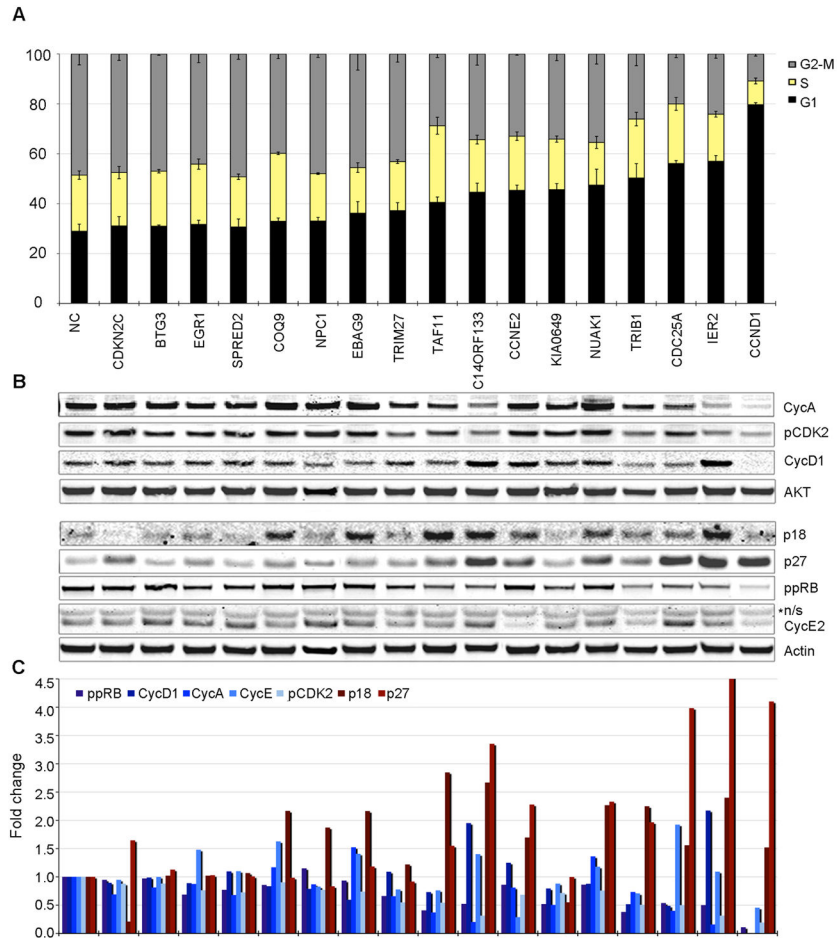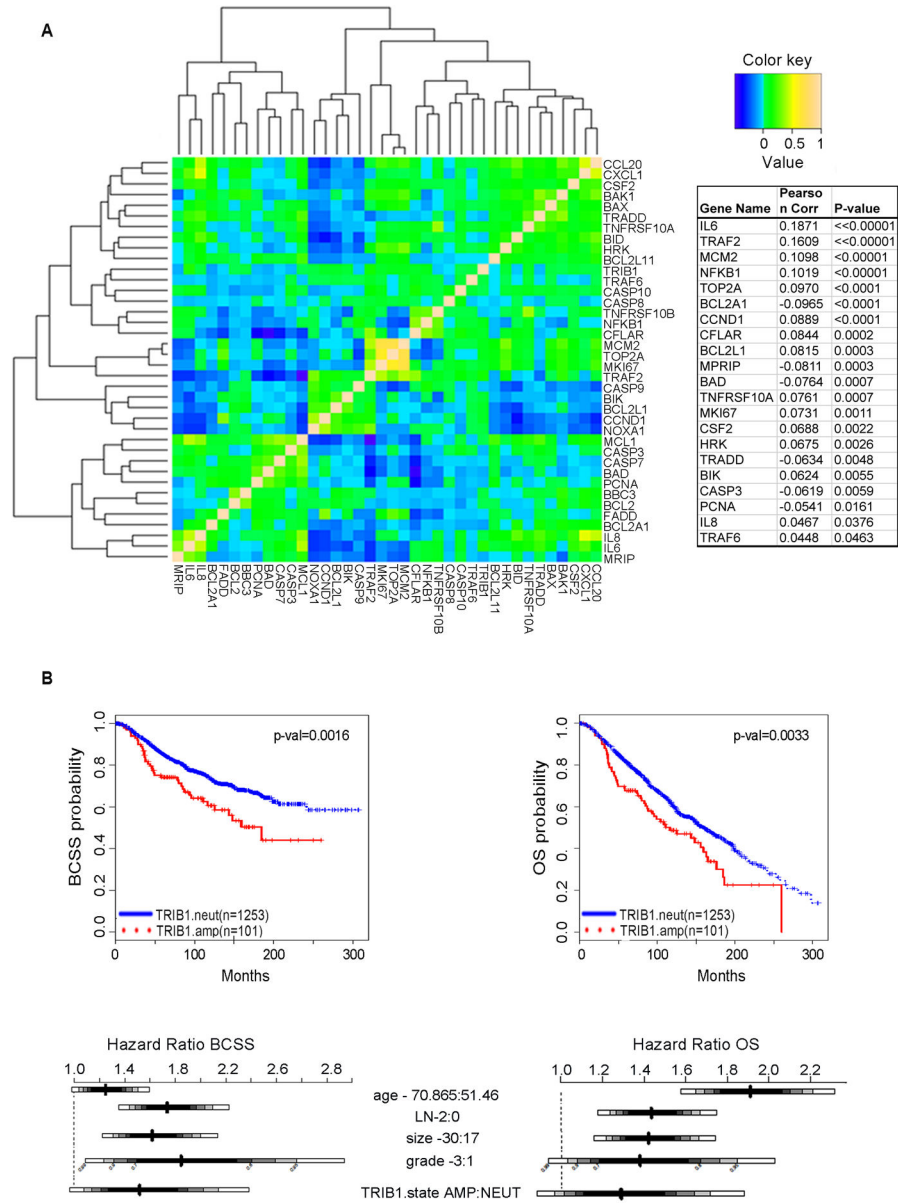
Figure 2.
Model validation: **A.** Cell cycle analysis of MDA-MB-231 cells treated with siRNA against 17 genes and NC siRNA. Cells were grown in DMEM-10%FBS, treated with designated siRNA pools and synchronized in G1 with mimosine. Cells were released from G1-block and cell cycle distribution was assessed by FACS at 10h post release. Data are shown as mean +/− standard deviation (sd) for three independent experiments. Statistical significance was determined by student t-test; * - p<0.05, ** - p<0.005, *** - p<0.0005; "+" designates genes predicted by the model to affect G1-S transition. **B–C.** Molecular inhibition of G1-S progression by KD. Cells were treated as in (a) and protein and phospho-protein levels were measured by immunoblotting (IB); n/s – non-specific band. Bands were normalized by total protein and plotted as fraction of NC-siRNA treatment.
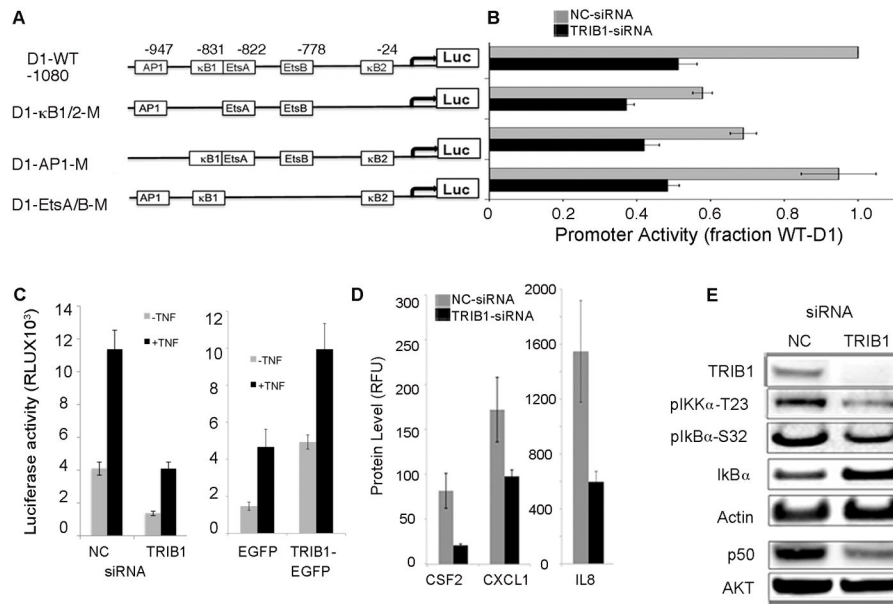
Figure 3.
TRIB1 mediates expression of CCND1 via regulation of NFκB and AP1. **A.** Schematic
representation of -1080-Cyclin D1 (D1) pGL3 basic luciferase reporter constructs and
deletion mutants. AP1, EtsA/B (both Ets A and B were deleted), and both NFκB sites (κB1
and κB2) were eliminated as shown. **B.** Cells were treated with NC or TRIB1 siRNA pools
for 24h followed by transfection with 1μg of CCND1-WT, AP1-mutant, EtsA/B-mutant, or
κB1/2-mutant promoter-reporter constructs. Luciferase activity was measured and
standardized by co-transfection with SEAP expression vectors. Results represent the means
and standard deviations from three independent experiments. (RLU, relative light units). **C.**
TRIB1 regulates NFκB-responsive promoter activity. Cells were treated as in (B) and
transfected with NFκB-responsive reporter vector and SEAP expression control vector, and
treated with TNFα for 4 h. Cells were co-transfected with 1μg vector-EGFP or TRIB1-
EGFP and with NFκB -promoter vector/SEAP and stimulated with TNFα for 4 h. **D.** TRIB1
knockdown leads to downregulation of NFκB target genes. Levels of CXCL1, CSF2, and
IL8 proteins were measured using Luminex assay for secreted cytokines. **E.** TRIB1
knockdown inhibits NFκB signaling via activation of IκBa and inhibition of p50 and
pIKKα. IB analysis of cells treated with NC or TRIB1 siRNA pools with indicated
antibodies.
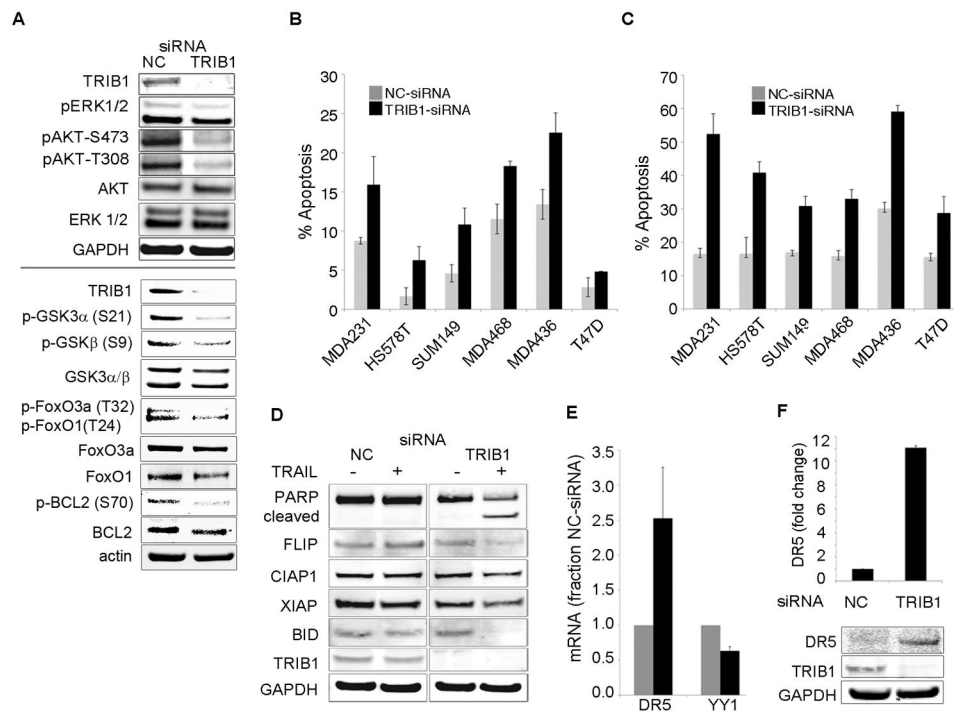
Figure 4.
TRIB1 knockdown induces apoptosis and sensitizes cells to TRAIL-induced apoptosis in breast cancer cells. **A.** TRIB1 knockdown inhibits ERK1/2 and AKT phosphorylation and activation of downstream signaling. IB analysis of cells treated with siRNA pools against NC or TRIB1 with indicated antibodies. **B**. MDA-MB-231, HS578T, SUM159, MDA-MB-468, MDA-MB-436, and T47D cells were transfected with NC (grey bars) or TRIB1 (black bars) siRNA pools, cells were stained with Annexin-V/PI and analyzed by FACS. Data shown as mean+/− sd of three independent experiments. **C**. TRIB1 knockdown sensitizes cells to TRAIL at non-lethal concentrations. Cells were treated as in (B) and followed by stimulation with TRAIL and analyzed as in (B). **D**. TRAIL–induced apoptosis occurs through inactivation of BCL2 and cleavage of BID. IB analysis of cells treated NC or TRIB1 siRNA −/+ TRAIL with indicated antibodies. **E**. Changes in YY1 and DR5 mRNA levels in response to TRIB1 siRNA. **F**. TRIB1 knockdown results in upregulation of DR5 protein.

Gene Name	Pearson Corr	P-value
IL6	0.1871	<<0.00001
TRAF2	0.1609	<<0.00001
MCM2	0.1098	<0.00001
NFKB1	0.1019	<0.00001
TOP2A	0.0970	<0.0001
BCL2A1	-0.0965	<0.0001
CCND1	0.0889	<0.0001
CFLAR	0.0844	0.0002
BCL2L1	0.0815	0.0003
MPRIP	-0.0811	0.0003
BAD	-0.0764	0.0007
TNFRSF10A	0.0761	0.0007
MKI67	0.0731	0.0011
CSF2	0.0688	0.0022
HRK	0.0675	0.0026
TRADD	-0.0634	0.0048
BIK	0.0624	0.0055
CASP3	-0.0619	0.0059
PCNA	-0.0541	0.0161
IL8	0.0467	0.0376
TRAF6	0.0448	0.0463

Figure 5.

Expression and survival analysis in primary tumors. **A.** Heatmap illustrating Pearson's correlation between the expression levels of a panel of 38 TRIB1, TRAIL, and NFkB associated genes in a cohort of primary breast tumors (n=1980). Genes that were significantly (p<0.05) associated with *TRIB1* expression are indicated in the accompanying table with their respective correlation coefficients. **B.** Kaplan-Meier and Hazard Ratio plots and log-rank p-values comparing breast cancer specific survival (BCSS) and overall survival (OS) distributions between individuals with *TRIB1* amplification in the upper (66.66%) versus lower (33.33%) tertiles.